Influence of correlations between scatterers on the attenuation of the coherent wave in a random medium

Arnaud Derode, Victor Mamou, and Arnaud Tourin
Laboratoire Ondes et Acoustique, Université Paris 7, ESPCI - CNRS, 10 rue Vauquelin, 75005 Paris, France
(Received 3 March 2006; revised manuscript received 7 July 2006; published 12 September 2006)

Experimental measurements of the coherent wave transmission for ultrasonic waves propagating in water through a random set of scatterers (metallic rods) are presented. Though the densities are moderate (6% and 14%) the experimental results show that the mean-free path deviates from the classical first-order approximation due to the existence of correlations between scatterers. Theoretical results for the mean free path obtained from different approaches are compared to the experimental measurements. The best agreement is obtained with the second-order diagrammatic expansion of the self-energy.

DOI: 10.1103/PhysRevE.74.036606 PACS number(s): 43.20.+g, 42.25.Dd, 43.35.+d, 46.65.+g

I. INTRODUCTION

Wave propagation in disordered media is an old subject that has undergone a tremendous revival in recent years [1–6]. Whatever the types of waves, a disordered scattering medium can be characterized by the spatial fluctuations of its physical properties, which are modeled as random processes. Given the relevant statistical parameters describing the medium, one tries to predict and measure the ensemble average of physical quantities such as the transmitted wave amplitude, intensity, flux, spatial, temporal, or spectral correlations, etc. Though the basic physical concepts in multiple wave scattering can be applied to whatever types of wave, the experimental advantage of acoustic waves is that wideband measurements of the field itself, and not only its intensity, are easily achievable with piezoelectric transducers.

In this paper, we present ultrasonic experimental measurements of the coherent wavefield [7–10], i.e., the ensemble-averaged field. Ultrasonic waves around 3 MHz are transmitted through scattering slabs containing discrete metallic scatterers immersed in water. The propagation of the coherent wavefield in a nondissipative random medium is characterized by an effective wave number k_{eff}, whose imaginary part accounts for the losses due to scattering. As the wave propagates in the medium, the intensity of its coherent part decays exponentially with a characteristic length $\ell_e = 1/(2\mathrm{Im}(k_{\mathrm{eff}}))$ termed the elastic mean-free path. For dilute media, the elastic mean-free path is usually well approximated by $\ell_e = 1/n\sigma$ with n the scatterer density and σ the scattering cross section of an individual scatterer. We focus here on the effect of spatial correlation between the scatterers. The experimental results show that even for moderate densities, the correlation resulting from steric repulsion between scatterers has a significant impact on the mean-free path, which is found to deviate by up to 25% from the first-order theoretical prediction $1/n\sigma$. To account for the experimental measurements, we compare several second-order explicit expressions for the effective wave number derived from earlier theoretical works. The Keller approach, based on a second-order diagrammatic expansion of the self-energy, is found to give the best agreement with the experimental results.

II. EXPERIMENTS

The coherent transmission experiment is depicted in Fig. 1. A piezoelectric element generates a short ultrasonic pulse (1 μs of a 3.2 MHz sine wave, average wavelength in water $\lambda = 0.47$ mm) that propagates through water and encounters a multiple scattering slab with thickness L. The slab consists of a random collection of parallel steel rods with diameter 0.8 mm. The concentration can be expressed either as a (dimensionless) surfacic fraction or as a number of scatterers per unit surface n. We have used two densities: $n=29$ and 12 rods/cm^2 which correspond to surface concentrations of 14% and 6%, respectively. The elastic parameters of the steel rods are $c_L = 5.7$ mm/μs, $c_T = 3$ mm/μs, and $\rho = 7.85$ kg/l. The rods are held together by two horizontal thin epoxy plates in which 0.8-mm holes were drilled at random positions. In order to avoid the overlapping of scatterers, an exclusion distance d was imposed between the holes centers: $d_{29} = 1.2$ mm and $d_{12} = 1.87$ mm, respectively. These values were chosen proportionally to the mean distance between scatterers $(1/\sqrt{n})$, and result in a partial correlation between scattering centers, the influence of which will be discussed in the next section. The receiving array has 128 0.39-mm large elements identical to the source element, with a 0.42 mm

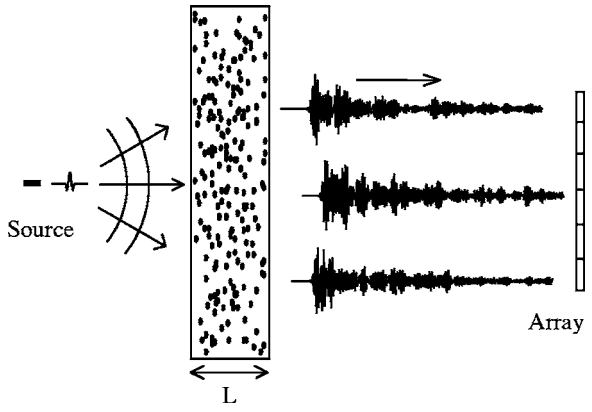

FIG. 1. The source transmits a short pulse that propagates through the slab. The scattered waves are recorded on a 128-element array. The sample can be translated parallel to the array for ensemble averaging.

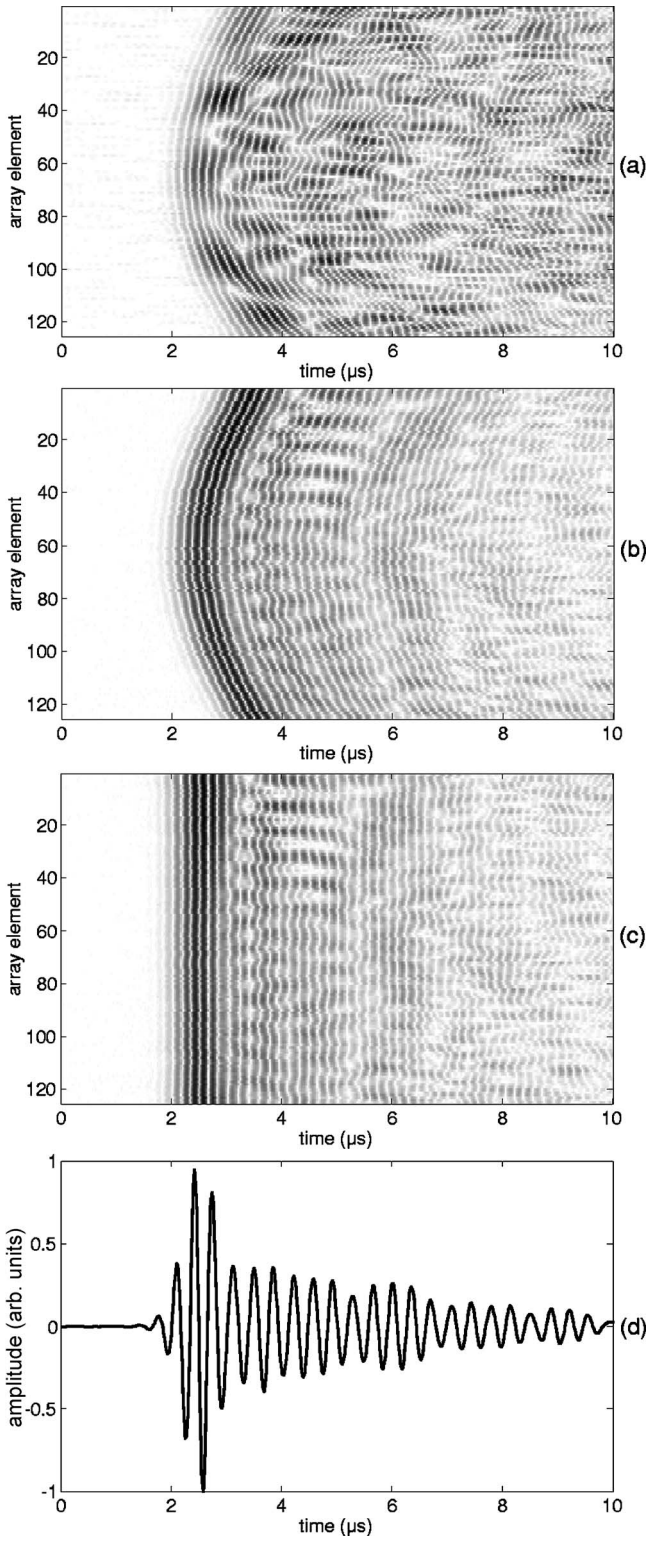

FIG. 2. Transmitted wavefield through a 15-mm thick slab with density 29.54 scatterers/cm^2: (a) one realization, (b) average over 100 positions, (c) same as (b) after time realignment, and (d) resulting coherent waveform. For (a)–(c) time is in the abscissa, and each line of the picture represents the magnitude of the signal received on one of the 128 array elements, in a linear grayscale. The signal in (d) is normalized to its maximum amplitude.

pitch. The elements are 10 mm in height and the setup is considered as two-dimensional. Scattered waves emerge from the slab and the array records 128 time series, as presented in Fig. 2. The signals are digitized over 12 bits at a 50 MHz sampling frequency. Rather than trying to give an exact analytical expression for this transmitted wave, it is a classical approach to describe the medium and the scattering process statistically. A given sample is considered as a particular realization of a random process, and the ensemble average of the transmitted field (also known as the coherent wave field) is considered. In the situation we study here, the scatterers positions are fixed and the ensemble average cannot be achieved experimentally by moving the scatterers, as is done naturally, e.g., in a scattering suspension. We simulate an ensemble average by translating both the source and the array parallel to the slab by several wavelengths; another wave field (128 time series) is acquired at the array. The procedure is repeated at 100 different positions, and the 100 wave fields are averaged to obtain an estimation of the *coherent wave front.* A typical example is shown in Fig. 2, in the case of a slab with thickness $L=15$ mm and density $n=29$ rods/cm^2. The average tends to reinforce the ballistic pulse contribution (i.e., the first arrival); it also appears that beyond the first arrival, persistent spatially coherent wave fronts have survived the average. This second contribution is due to the individual resonances of the scatterers [7] and its frequency spectrum differs significantly from that of the ballistic front. The next step consists in time-shifting these 128 time series (Fig. 2) to align them in phase (naturally, this operation makes sense only if a well-defined wave front emerges after averaging). Then the time-shifted signals are averaged to form the coherent wave form $u_C(L,t)$. This wave form is compared to that obtained under the same conditions in water without the scattering slab ($L=0$). The transmission coefficient for the coherent energy is evaluated by

$$T_C(L) = \frac{\int u_C^2(L,t)dt}{\int u_C^2(0,t)dt} = \frac{\int |U_C(L,\omega)|^2 d\omega}{\int |U_C(0,\omega)|^2 d\omega} \qquad (1)$$

with U the Fourier transform of u. When necessary, the spectra are integrated in narrow frequency bands (0.1 MHz wide) to obtain the frequency dependence of the transmission coefficient.

The extinction of the coherent wave results from two different physical phenomena, scattering and absorption. It is well-known that the intensity of the coherent wave decreases with thickness as $\exp(-K_{ext}L)$, with K_{ext} the extinction coefficient related to the elastic mean-free path ℓ_e and to the absorption mean-free path ℓ_a: $K_{ext}=\frac{1}{\ell_e}+\frac{1}{\ell_a}$. With the normalization procedure we employed [Eq. (1)], the measured transmission coefficient $T_C(L)$ is independent from the intrinsic absorption length in water. Moreover, the additional absorption at the scatterer/water interface was found negligible [11–13]. Therefore the decrease of the experimental coherent transmission coefficient $T_C(L)$ with L gives a direct measurement of the elastic mean-free path, free from intrinsic ab-

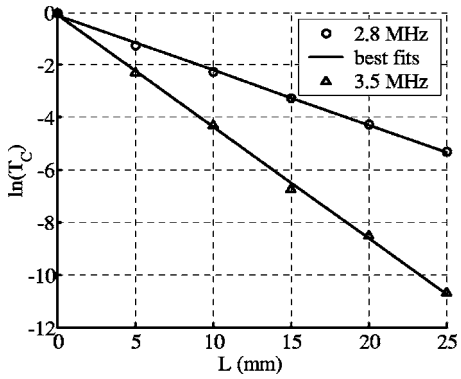

FIG. 3. Coherent transmission through the most dense slabs ($n=29.54$ cm^{-2}). Measurements of the transmission coefficient vs thickness, at 2.8 and 3.5 MHz.

sorption. A least-squares linear fit of $\ln(T_C)$ provides an estimate for ℓ_e and its standard deviation. The wideband values of ℓ_e are 7.7 ± 0.3 and 3.15 ± 0.15 mm, respectively, for the two concentrations. However, these wideband values hide the variations of ℓ_e with frequency, which appear to be important (Figs. 3 and 4) as one could expect. The elastic mean-free path strongly depends on frequency; in both samples, the experimental results show that ℓ_e can vary by more than a factor of 2 in the 2–4 MHz frequency range.

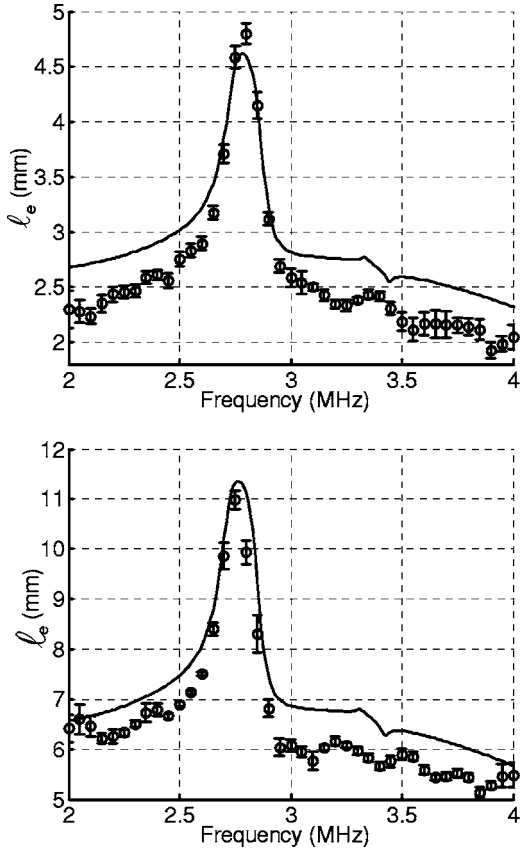

FIG. 4. Variation of the mean-free path with frequency for $n=29.54$ cm^{-2} (top) and $n=12$ cm^{-2} (bottom). Circles: experimental measurement ± one standard deviation. Continuous line: first-order theoretical prediction (ISA).

These results are consistent with previous studies which showed that the total scattering cross section σ of the steel rods is weaker around 2.7 MHz because of an elastic resonance; this makes the slab less scattering hence more transparent around this frequency [7].

Even though the surfacic fractions are moderate (6% and 14%) the usual approximation $\ell_e=1/n\sigma$ does not correctly fit the data (Fig. 4). The discrepancy is particularly obvious for small values of ℓ_e: for instance, in the most concentrated slab between 3 and 4 MHz there is a difference of up to 25% (corresponding to several standard deviations) between theory and experiments. Except around the resonance (2.5–2.9 MHz) where the approximation $\ell_e=1/n\sigma$ appears to fit the data reasonably, the actual mean-free path is systematically overestimated, and this difference cannot be explained by intrinsic absorption as we have argued. We think it is linked both to the concentration and the correlation between scattering centers. In the next section we try several second-order theoretical expressions of the effective wave number to account for the experimental results.

III. THEORETICAL APPROACHES

In the following, we omit the time-dependence of harmonic waves $e^{-j\omega t}$. When a scalar plane wave $e^{j\vec{k}_0\cdot\vec{r}}$ impinges on an elastic cylinder located at the origin, the far-field solution at $\vec{r}$ is written

$$e^{j\vec{k}_0\cdot\vec{r}}+f(\vec{k}_0,\vec{k}')\frac{e^{jk_0r}}{\sqrt{r}}.$$

The scattering cross section is

$$\sigma=\int_0^{2\pi}|f(\theta)|^2d\theta$$

with $\theta=(\vec{k}_0,\vec{k}')$ the scattering angle and f the scattering amplitude. Alternatively, other authors refer to a scattering matrix t linking the incoming $(\vec{k}_0)$ and the outgoing $(\vec{k}')$ wave vector. Here we will express the results in terms of the scattering matrix t rather than the amplitude f. In two dimensions [2], the scattering matrix and the scattering amplitude are related by

$$t(\vec{k}_0,\vec{k}')=-\sqrt{8\pi k_0}e^{-i\pi/4}f(\vec{k}_0,\vec{k}')$$

The scattering amplitude f or the scattering matrix t for an elastic cylinder can be expressed as a modal sum [14] and calculated numerically.

When dealing with multiple scattering through an inhomogeneous (but statistically homogeneous) slab, one tries to evaluate the effective wave number k_{eff} of the ensemble-averaged transmitted field. The elastic mean-free path is related to the imaginary part of k_{eff}, while the real part determines the speed of the coherent wave. In general, the exact calculation of k_{eff} is untractable, but different approaches and approximations have been used. Most of them derive from Foldy [15]. It is out of the scope of this paper to re-establish his (and following) results, but we briefly recall the fundamental ideas (see, e.g., Ref. [16] for a thorough analysis of Foldy's and Lax's works).

The complex wave field resulting from scattering of an incoming plane wave $\psi_0(\vec{r})=e^{j\vec{k}_0\cdot\vec{r}}$ on an ensemble of discrete isotropic point scatterers may be written as the sum of the incident wave plus the contribution from every scatterer, each contribution being proportional to the field exciting the scatterer:

$$\psi(\vec{r}) = \psi_0(\vec{r}) + \sum_j g_j \psi^j(\vec{r}_j) G_0(\vec{r},\vec{r}_j).$$

In this expression $\psi^j(\vec{r}_j)$ denotes the external field acting on the jth scatterer, g_j characterizes the strength of this scatterer, and G_0 is the Green's function of the homogenous embedding medium. The external field itself may be written as

$$\psi^j(\vec{r}_j) = \psi_0(\vec{r}_j) + \sum_{k\neq j} g_k \psi^k(\vec{r}_k) G_0(\vec{r}_j,\vec{r}_k).$$

From this couple of equations, Foldy calculated the ensemble-averaged field under the essential approximation that the external field acting on the jth scatterer remains the same whether this scatterer is held fixed or not

$$\langle \psi^j(\vec{r})\rangle_j \approx \langle \psi^j(\vec{r})\rangle.$$

This is valid if conditional (*a posteriori*) and unconditional (*a priori)* probabilities are identical, which, from a physical point of view, means that the scatterers positions do not influence one another, like molecules of a perfect gas. Under this hypothesis, the effective wave number is found to be

$$k_{eff}^2 = k_0^2 - nt(\vec{k}_0,\vec{k}_0).$$

The backscattered amplitude and the scattering cross section are related by the optical theorem $\sigma=-\mathrm{Im}\{t(\vec{k}_0,\vec{k}_0)\}/k_0$ [2]. Usually $n|t(\vec{k}_0,\vec{k}_0)|$ is much smaller than k_0^2 and the square root of the previous equation can be linearized into

$$k_{eff} \approx k_0 - nt(\vec{k}_0,\vec{k}_0)/2k_0.$$

Precisely, in our two-dimensional (2D) case for the resulting error to be smaller than 1% this condition requires the concentration n to be less than $0.25\pi/|f(0)|\lambda^{3/2}$ ~ 230 scatterers/cm^2 at 3 MHz which is largely verified here. One then finds the well-known result

$$\ell_e = 1/(2\mathrm{Im}(k_{\mathrm{eff}})) \approx 1/n\sigma.$$

Similarly to Foldy's assumption, the quasicrystalline approximation (QCA) [16–20] consists of assuming that $\langle \psi^j(\vec{r})\rangle_{j,k} \approx \langle \psi^j(\vec{r})\rangle_j$. To the first order in n, it gives the same expression for the effective wave number.

Subsequent works [21,22] yielded refined explicit expressions for k_{eff} (hence the mean-free path) up to the second order in n. Waterman and Truell (WT) obtained the following result:

$$k_{eff}^2 = k_0^2 - nt(\vec{k}_0,\vec{k}_0) + n^2\{t^2(\vec{k}_0,\vec{k}_0) - t^2(\vec{k}_0,-\vec{k}_0)\}/4k_0^2.$$

Lloyd and Berry [22] revised Waterman and Truell's expression and proposed a corrected second-order expression in three dimensions. Recently in a remarkable paper [16], Linton and Martin (LM) analyzed thoroughly Foldy's assumption and the QCA; they derived another explicit expression

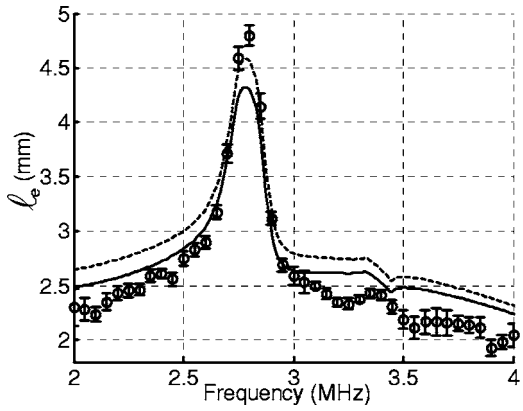

FIG. 5. Variation of the mean-free path with frequency for $n=29.54$ cm^{-2}. Circles: experimental measurement ± one standard deviation. Continuous line: Linton and Martin's result, and dashed line: Waterman and Truell's.

for k_{eff} in two dimensions, based on the QCA and the "hole correction" and assuming that the exclusion distance d is small compared to the wavelength:

$$k_{eff}^2 = k_0^2 - nt(\vec{k}_0,\vec{k}_0) - \frac{n^2}{2\pi k_0^2}\int \tan^{-1}\frac{\theta}{2}\frac{d}{d\theta}t^2(\theta)d\theta. \quad (2)$$

Nonexplicit formulations for k_{eff} have also been established, based on the QCA and the hole correction [19,20].

We have computed numerically the mean-free path from WT and LM expressions, the result is plotted in Fig. 5. There is no visible difference between WT and the first-order approximation $\ell_e=1/n\sigma$, which is clearly inappropriate to account for the experimental results. On the contrary, LM's expression is closer to the experimental results, which is quite remarkable since Eq. (2) is only valid in the limit $kd \to 0$ while in our experiments $kd \sim 10-30$. Yet the remaining discrepancy is still significant.

A key parameter, besides the concentration n, is the correlation between scatterers. Here the existence of a correlation between the scattering centers is due to the exclusion distance d, which is larger than the diameter of the rods. Mathematically, correlations are usually characterized by the radial distribution function g defined such that $ng(r)$ is the mean concentration at a distance r from a scatterer. Alternatively, one may refer to the pair correlation function $1-g(r)$. For an ensemble of pointlike noninteracting particles like in an ideal perfect gas, one has $g(r)=1\,\forall\, r$. If there is a steric repulsion with an exclusion distance d between scatterers, the "hole correction" approximation consists in writing:

$$g(r) = \begin{cases} 0, & r < d \\ 1, & r \geq d. \end{cases}$$

However, the "hole correction" does not describe the correlation properly. For scatterers picked at random with a given density n and an exclusion distance d, the radial distribution function is 0 for $r<d$ but oscillates for r ranging between d and $\sim 3d$ before reaching a plateau. An analytical expression for these oscillations can be obtained via the Perkus-Yevick

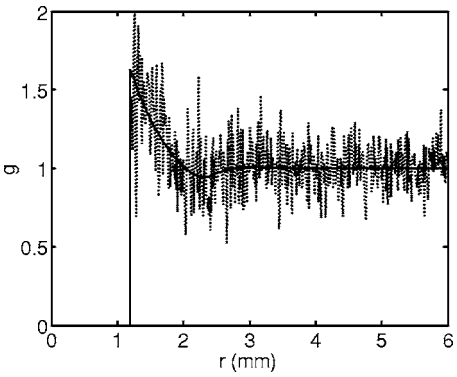

FIG. 6. Dashed line: radial distribution function estimated from one realization (2000 scatterers with density $n=29.54$ cm^{-2} and exclusion distance $d=1.2$ mm). Continuous line: average for 20 000 realizations.

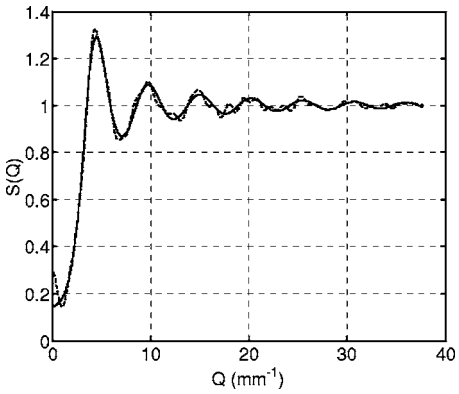

FIG. 7. Dimensionless structure factor S(Q) computed from the radial distribution functions plotted in Fig. 6. One realization (dotted line), average over 20 000 realizations (continuous line).

approximation [23,24], but it is quite complicated and is still only an approximation for $g(r)$. In our case, the coordinates (x_j,y_j) of each scatterer have been picked by a random number generator, with a uniform distribution for x and y, and with the condition that no pair of scatterers could be closer than d. Since we have the coordinates of each scattering center, we can estimate $g(r)$ by building a histogram of the number of scatterers whose distance from a given scatterer is comprised between 0 and r, and averaging for every possible origin scatterer. The resulting function is plotted in Fig. 6 for one realization, as well as for the average of 20 000 realizations. The average curve is similar to those obtained under the Perkus-Yevick approximation [24].

Once the radial distribution function $g(r)$ is known (or modeled) there are different approaches to take it into account explicitly in the calculation of the mean-free path. To the first order in n, an approximation sometimes referred to as the interference approximation (ITA) [25–28] consists in replacing the scattering cross section σ by

$$\sigma_c = \int_0^{2\pi} |f(\theta)|^2 S(\theta) d\theta,$$

with S the static structure factor, related to the spatial Fourier transform of the radial distribution function:

$$q = 2k_0 \sin(\theta/2),$$

$$S(q) = 1 - n \int [1 - g(r)] e^{i\vec{r}\cdot\vec{q}} d\vec{r}.$$

The structure factor and the corrected cross section σ_c have been evaluated by numerical integration and plotted in Figs. 7 and 8. Here the effect of the structure factor is to lower the scattering cross section by roughly 25%, which makes the medium more transparent. This has also been reported in previous works in optics [25,26]. However, in our case the ITA does not fit the experimental observation at all, the discrepancy between first-order corrected theory $(1/n\sigma_c)$ and the experimental mean-free path being even larger than under Foldy's assumption.

Another family of approaches, different from Foldy's, the QCA, or the ITA, is based on diagrammatic representations and classification of multiple scattering events [2,29,30]. Again, it is out of the scope of this paper to give a detailed account of the diagrammatic theory of multiple scattering but we give here a very brief overview. For monochromatic waves, the scalar wave equation in a heterogeneous medium may be written

$$\Delta\Psi(\vec{r}) + k_0^2\Psi(\vec{r}) = V(\vec{r})\Psi(\vec{r})$$

with V the "potential" characterizing the deviations from the homogeneous medium with wave number $k_0=\omega/c_0$.

The Green's function G satisfies the equation

$$\Delta G(\vec{r},\vec{r}') + k_0^2 G(\vec{r},\vec{r}') = V(\vec{r})G(\vec{r},\vec{r}') + \delta(\vec{r}-\vec{r}').$$

Its solution may be written

$$G(\vec{r},\vec{r}') = G_0(\vec{r}-\vec{r}') + \int G_0(\vec{r}-\vec{r}_1)V(\vec{r}_1)G(\vec{r}_1,\vec{r}')d\vec{r}_1.$$

Introducing a two-entry operator $V(\vec{r}_1,\vec{r}_2)=V(\vec{r}_1)\delta(\vec{r}_1-\vec{r}_2)$, we have

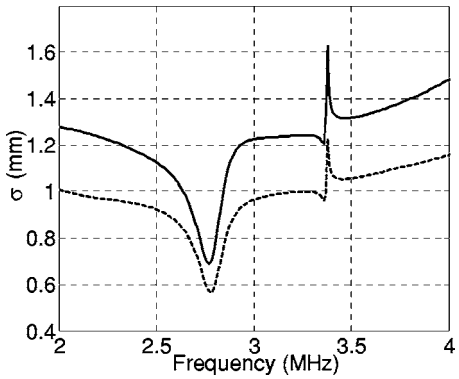

FIG. 8. Continuous line: scattering cross section σ for a steel cylinder with radius 0.4 mm. Dashed line: corrected scattering cross section σ_c.

$$G(\vec{r},\vec{r}') = G_0(\vec{r}-\vec{r}') + \int\int G_0(\vec{r}-\vec{r}_1)V(\vec{r}_1,\vec{r}_2)G(\vec{r}_2,\vec{r}')d\vec{r}_1 d\vec{r}_2,$$

which can be condensed into a matrix product:

$$G = G_0 + G_0 V G.$$

This is the closed-form expression for the Green's function G. If we reinject G in the right-hand side, we obtain the well-known Born expansion:

$$G = G_0 + G_0 V G_0 + G_0 V G_0 V G_0 + \cdots,$$

which can be interpreted as a sum of an homogeneous term, a single scattering term, a double scattering term, and so on.

The Born expansion may also be wrapped up as

$$G = G_0 + G_0 T G_0$$

with T the scattering operator such that

$$T = V + V G_0 V + V G_0 V G_0 V + \cdots.$$

For the case of a single scatterer, the scattering operator is simply the scattering matrix t that we mentioned earlier.

Naturally, these relations can also be expressed in the spatial frequency space via a Fourier transform. At this stage, the Green's function can be expressed either as an infinite sum (Born series) or in a closed-form solution. Similarly, the ensemble-averaged Green's function $\langle G \rangle$ obeys

$$\langle G \rangle = G_0 + G_0 \langle T \rangle G_0, \tag{3}$$

which can be rearranged under a closed-form expression, known as Dyson's equation:

$$\langle G \rangle = G_0 + G_0 \Sigma \langle G \rangle, \tag{4}$$

Σ is called the mass operator, or the field kernel, or the self-energy. The medium is supposed to be statistically stationary and invariant under rotation, so Σ and $\langle G \rangle$ only depend on $|\vec{r}_1-\vec{r}_2|$ and their 6D-Fourier transforms will be written in the form $F(|\vec{k}_1|)\delta(\vec{k}_1-\vec{k}_2)$. Hence the Fourier transform of Dyson's equation gives a simple product in the k-space whose solution is

$$\langle G \rangle = \frac{G_0}{1-\Sigma G_0}.$$

The effective wave number k_{eff} can be easily expressed in terms of Σ. Since we have $G_0 = 1/(k_0^2-k^2)$ in the $\vec{k}$-space, it is convenient to rewrite the average Green's function as $\langle G \rangle = 1/(k_{eff}^2-k^2)$, with by identification $k_{eff}^2 = k_0^2 - \Sigma$.

Of course, the main difficulty lies in the exact computation of the self-energy. In the diagrammatic approach, in order to avoid lengthy expressions with multiple integrals and keep a physical picture of the scattering process, the important quantities like the scattering operator T, the average Green's function $\langle G \rangle$, and the self-energy Σ are schematically represented as a sum of diagrams. The diagrammatic development for $\langle G \rangle$ is represented in Fig. 9. The conventions [29,30] we follow here are

(1) a crossed circle symbolizes the scattering by one scatterer, averaged over disorder;

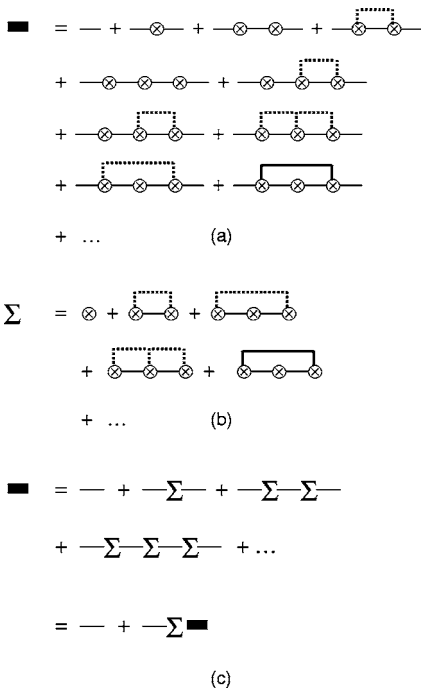

FIG. 9. Diagrammatic representations of multiple scattering. (a) The average Green's function is written as a sum of diagrams similar to a Born expansion represented here up to the third order. (b) The sum of *strongly connected* diagrams appearing in (a) is denoted Σ. (c) The development of the average Green's function can then be rewritten introducing Σ, and wrapped up as a closed form: Dyson's equation.

(2) a thick horizontal line represents the average Green's function;

(3) a thin horizontal line represents the homogeneous Green's function G_0;

(4) dotted lines relate correlated scatterers; and

(5) continuous lines relating two circles indicate that they represent the same scatterer.

All the diagrams of Fig. 9(a) may be rearranged according to their connexity. A diagram is said to be strongly connected if it cannot be decomposed into simpler diagrams without cutting a line other than the base line. All strongly connected diagrams may be gathered in a sum, which is represented in Fig. 9(b). The advantage of this classification is that the average Green's function may be written in a closed form solution [Fig. 9(c)]. By identification with Eq. (4), the self-energy now *explicitly* appears as the sum of strongly connected diagrams (Fig. 9). Thus the self-energy is organized in a well-hierarchized sum of easily identifiable terms.

At that point, several approximations can be made. The simplest is to assume that the scatterers are completely decorrelated and neglect "loops" (which implies that each scatterer is visited by the wave at most once). In the literature, this approximation is referred to as the ISA (independent scattering approximation). Under the ISA, only the first term remains in the development of the self-energy, which leads to

$$\Sigma = nt(\vec{k}_0,\vec{k}_0).$$

This yields exactly the same expression for the effective wave number as Foldy's:

$$k_{eff}^2 = k_0^2 - nt(\vec{k}_0, \vec{k}_0).$$

Interestingly, loops only appear as a *third-order* correction in the development of the self-energy, as was already pointed out by Henyey [31] following a diagrammatic approach. But spatial correlations between scatterers are of second order, and should be taken into account before loops. The second order term in the diagrams of Fig. 9(b) can be calculated following Keller's approach [32], assuming that the scatterers are small compared to the wavelength. In 2D, this yields the following expression where the radial distribution function $g(r)$ explicitly appears as a second-order correction:

$$k_{eff}^2 = k_0^2 - nt(\vec{k}_0, \vec{k}_0) - n^2 t^2(\vec{k}_0, \vec{k}_0) \int_0^\infty \frac{i\pi}{2} H_0^1(k_0 r) J_0(k_{eff} r) \times [1 - g(r)] r dr. \quad (5)$$

Note that the effective wave number k_{eff} appears on both sides of the equation; we computed k_{eff} following an iterative procedure. We used as a first approximation the effective wave number given by the ISA, k_{ISA}. We evaluated the integral in the right-hand side of Eq. (5) to obtain a new value for k_{eff}, and repeated the procedure. It was found to converge very rapidly (typically less than five iterations for the concentrations and frequencies we studied); in fact, in the situations we studied here, if we simply replace k_{eff} by k_{ISA} in the right-hand side of Eq. (5), the resulting error for the mean-free path is always less than 0.2%. In such a case Eq. (5) can be transformed into an explicit expression for k_{eff}. Theoretical results based on Eq. (5) are compared to the experimental values of ℓ_e in Fig. 10. This time, we observe that the agreement is excellent. The same agreement is obtained with other slabs ($n=18.75$ cm^{-2}) containing smaller scatterers (diameter 0.6 mm) that resonate at a higher frequency (Fig. 10).

A numerical comparison between the experimental results and the theoretical predictions for both concentrations is given in Table I. Note that for 3D optical waves in latex suspensions of spherical particles [33,34], Keller's second-order perturbative result was also found to predict the attenuation constant of the coherent field better than other approaches, even for particles with a radius exceeding the wavelength, but for low dielectric contrasts. Here, the acoustic impedance mismatch between water and steel is roughly 30.

The effect of the second-order term on the sound velocity has also been studied. It appears to be much smaller than for the mean-free path. Even in the most concentrated slabs, the difference between first- and second-order theoretical results do not exceed 0.5% on the phase velocity and 5% on the group velocity; the difference reaches its maximum near the resonance frequency (2.8 MHz). Experimentally, the group velocity was measured in the most concentrated slabs, for four different thicknesses (Fig. 11). The group velocity was found to differ very significantly from the sound velocity in water around the resonance. This is in agreement with previous results [7–10], and is due to the larger "dwell time" (group delay) at the resonance which slows down the incoming wave packet, as if the wave was trapped by the resonating scatterers. At 2.8 MHz, the experimental results are in better agreement with the predictions from the second-order diagrammatic approach, however, the experimental error bars are too large to honestly discriminate between the first- and second-order theoretical results.

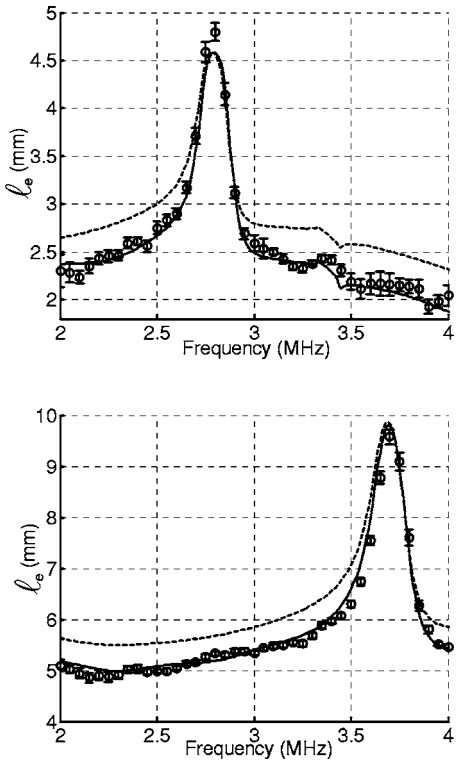

FIG. 10. Variation of the mean-free path with frequency for $n=29.54$ cm^{-2}, diameter 0.8 mm (top) and $n=18.75$ cm^{-2}, diameter 0.6 mm (bottom). Circles: experimental measurement ± one standard deviation. Dashed line: ISA. Continuous line: second-order diagrammatic approach (Keller).

IV. CONCLUSION

To the first order in n, there is no difference between the various theoretical approaches we have studied. There is, however, a conceptual difference between Foldy's approach,

TABLE I. Mean relative difference between theory and experiments in the 2–4 MHz band, for three types of scattering slabs. ISA=independent scattering approximation, WT=Waterman and Truell, LM=Linton and Martin, K=Keller second-order diagrammatic approach, and Exp=average experimental standard deviation.

	$n=12$ cm^{-2} diameter 0.8 mm (%)	$n=29.54$ cm^{-2} diameter 0.8 mm (%)	$n=18.75$ cm^{-2} diameter 0.6 mm (%)
ISA	9.2	13.7	9.0
WT	8.9	13.2	8.6
LM	6.8	8.9	6.6
K	3.5	3.5	2.0
Exp	2.1	3.0	1.3

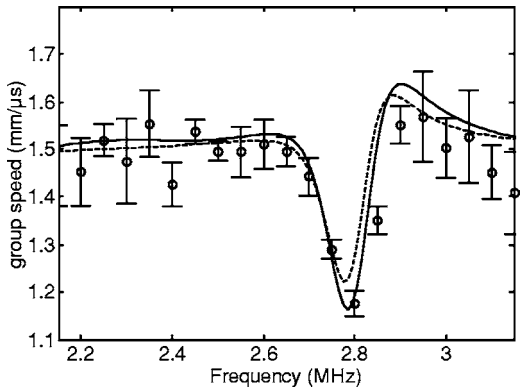

FIG. 11. Group speed vs frequency for a scattering slab with $n=29.54$ cm^{-2}, diameter 0.8 mm. Circles: experimental measurements averaged over four slab thicknesses ± one standard deviation. Dashed line: ISA. Continuous line: second-order diagrammatic approach (Keller).

Waterman and Truell's, or the QCA on the one hand and the diagrammatic approach on the other hand. The former are founded on mathematical hypotheses regarding the "external field" $\psi^j(\vec{r})$; the repulsion between scatterers can also be incorporated as an ingredient, but it is not easy to identify which physical phenomena are neglected under these hypotheses. Whereas the diagrammatic approach shows that the coherent wave field is entirely determined by the self-energy and allows one to develop Σ in a well-organized series of terms, each of them being represented by a diagram. Therefore one can identify what kind of contributions (e.g., loops, interactions between two or more correlated scatterers,…) are neglected when the development is truncated at some order.

The experimental results we presented show that even in relatively tenuous media (6%–14%, and $n|t| \ll k_0^2$) the second order term is necessary to calculate the mean-free path, not so much because of the scatterer density but because of the correlation induced by the repulsion between scatterers. If necessary, higher order terms (accounting for loops, correlation between n-uplets of scatterers, etc.) could be incorporated, at the cost of a loss of simplicity. Actually the expression for k_{eff}^2 derived from the diagrammatic approach can be seen as a perturbative result with nt/k_0^2 as a small parameter that converges as long as it remains small. When it is no longer small, or when scatterers are so strongly correlated that high-order terms are necessary, the diagrammatic approach is of less interest. In dense scattering media, for instance, other approaches would be more suitable, such as the CPA (coherent potential approximation [2,8–10]) which was shown to adequately describe experimental measurements in very dense packings of spheres (volume fraction ~60%). Here we illustrated the fact that even in a medium that can be considered as dilute, very far from the close-packing limit, scatterer correlations play an important role and classical corrections such as Waterman and Truell's or the ITA fail while Linton and Martin's (based on the QCA) and mostly Keller's (based on the diagrammatic approach) give much better results, though they result in explicit and easily computable formulations for the effective wave number.

ACKNOWLEDGMENT

The authors wish to thank R. Maynard, M. Fink, B. van Tiggelen, and J.H. Page for numerous discussions, as well as S. Durant for his advice.

[1] Ping Sheng, *Scattering and Localization of Classical Waves in Random Media* (World Scientific, Singapore, 1990).
[2] Ping Sheng, *Introduction to Wave Scattering, Localization and Mesoscopic Phenomena* (Academic Press, New York, 1995).
[3] A. Ishimaru, *Wave Propagation and Scattering in Random Media* (Academic Press, New York, 1978), Vols. I and II.
[4] A. Lagendijk and B. van Tiggelen, Phys. Rep. **270**, 143 (1996).
[5] S. Skipetrov and B. van Tiggelen, *Wave Scattering in Complex Media: From Theory to Applications*, NATO Science Series (Kluwer, Dordrecht, 2003), Vol. 107.
[6] R. Snieder, in *Diffuse Waves in Complex Media* (Kluwer, Dordreecht, 1999), p. 405.
[7] A. Derode, A. Tourin, and M. Fink, Phys. Rev. E **64**, 036605 (2001); A. Tourin, A. Derode, A. Peyre, and M. Fink, J. Acoust. Soc. Am. **108**, 503 (2000).
[8] J. H. Page, H. P. Schriemer, I. P. Jones, P. Sheng, and D. A. Weitz, Physica A **241**, 64 (1997); J. H. Page, P. Sheng, H. P. Schriemer, I. Jones, X. Jing, and D. A. Weitz, Science **271**, 634 (1996).
[9] M. L. Cowan, K. Beaty, J. H. Page, Z. Liu, and P. Sheng, Phys. Rev. E **58**, 6626 (1998).
[10] Z. Q. Zhang, I. P. Jones, H. P. Schriemer, J. H. Page, D. A. Weitz, and P. Sheng, Phys. Rev. E **60**, 4843 (1999).
[11] W. H. Lis and A. C. Raptis, J. Acoust. Soc. Am. **74**, 1542 (1983).
[12] A. E. Hay and R. W. Burling, J. Acoust. Soc. Am. **72**, 950 (1982).
[13] G. C. Gaunaurd, J. Acoust. Soc. Am. **62**, 503 (1977).
[14] L. Flax, G. C. Gaunaurd, and H. Überall, in *Physical Acoustics* Vol. XV (Academic Press, New York, 1981).
[15] L. Foldy, Phys. Rev. **67**, 107 (1945).
[16] C. M. Linton and P. A. Martin, J. Acoust. Soc. Am. **117**, 3413 (2005).
[17] M. Lax, Phys. Rev. **85**, 621 (1952).
[18] R. West, D. Gibbs, L. Tsang, and A. K. Fund, J. Opt. Soc. Am. A **11**, 1854 (1994).
[19] V. N. Bringi and V. V. Varadan, Radio Sci. **17**, 946 (1982).
[20] P-Y. Le Bas, F. Luppé, and J.-M. Conoir, J. Acoust. Soc. Am. **117**, 1088 (2005); Y. C. Angel and C. Aristégui, *ibid.* **118**, 72 (2005).
[21] P. C. Waterman and R. Truell, J. Math. Phys. **2**, 512 (1961).
[22] P. Lloyd and M. V. Berry, Proc. Phys. Soc. London **91**, 678 (1967).
[23] J. K. Percus and G. J. Yevick, Phys. Rev. **110**, 1 (1958).
[24] L. Tsang, J. A. Kong, and T. Habashy, J. Acoust. Soc. Am. **71**,

552 (1982).
[25] P. M. Saulnier, M. P. Zinkin, and G. H. Watson, Phys. Rev. B **42**, R2621 (1990).
[26] V. P. Dick and A. P. Ivanov, J. Opt. Soc. Am. **16**, 1034 (1999).
[27] S. Fraden and G. Maret, Phys. Rev. Lett. **65**, 512 (1990).
[28] P. D. Kaplan, A. D. Dinsmore, A. G. Yodh, and D. J. Pine, Phys. Rev. E **50**, 4827 (1994).
[29] U. Frisch, in *Probabilistic Methods in Applied Mathematics*, edited by A. T. Bharucha-Reid (Academic Press, New York, 1968), Vol. 1, p. 75.
[30] Yu. A. Kravtsov, S. M. Rytov, and V. I. Tatarskii, *Principle of Statistical Radiophysics* (Springer-Verlag, Berlin, 1989).
[31] F. S. Henyey, J. Acoust. Soc. Am. **105**, 2149 (1999).
[32] J. Keller,Proc. Symp. Appl. Math. **16**, 145 (1964); S. Durant, Ph.D. dissertation (in French), Ecole Centrale de Paris, 2003.
[33] A. Ishimaru and Y. Kuga, J. Opt. Soc. Am. **72**, 1317 (1982).
[34] L. Hespel, S. Mainguy, and J.-J. Greffet, J. Opt. Soc. Am. A **18**, 3072 (2001).